Chapter 3 *Structural Transformation and Bandgap Engineering by Doping Pr in Nanoparticles of HfO_2*

3.1 Introduction

In this chapter, we have stabilized the high temperature cubic phase of HfO_2 at room temperature with doping praseodymium (Pr) up to 15 at%. While monoclinic phase remains stable below 7 at%, coexistence of monoclinic and cubic phases is observed between 7 and 13 at% of Pr. Doping Pr in HfO_2 increases the oxygen vacancies which induce 8-fold oxygen coordinated Pr^{3+} ions in the lattice to stabilize the cubic phase. The structural and microstructural analysis is given in the sections 3.2.1 to 3.2.3. The mechanism of phase transformation from monoclinic to cubic phase is described in the section 3.2.4. The optical bandgap tuning after doping Pr is discussed in section 3.3. Bandgap decreases from 5.42 to 5.06 eV due to formation of sub-bands near conduction band because of enhanced oxygen vacancies. The important results of this chapter are summarized in section 3.4.

3.2 Structure, Microstructure and Phase Transformation

3.2.1 XRD, Raman Spectroscopy and FTIR Spectroscopy

We have investigated the structure and phase transformation of HfO_2 nanoparticles by doping Pr through X-ray diffraction (XRD) and Raman spectroscopy. **Figure 3.1** depicts XRD patterns of $Hf_{1-x}Pr_xO_2$ ($0 \leq x \leq 0.15$) nanoparticles. For $x = 0$, the sharp diffraction peaks are indexed as the monoclinic phase of HfO_2 ($P2_1/c$, JCPDS file number 78–0049). At $x = 0.01$, the diffraction pattern is almost identical to the monoclinic phase whereas,

at x = 0.07, the diffraction pattern contains a weak peak at ~ 30.2° ascribed to (111) of cubic phase ($Fm\bar{3}m$, JCPDS file number 53–0560).

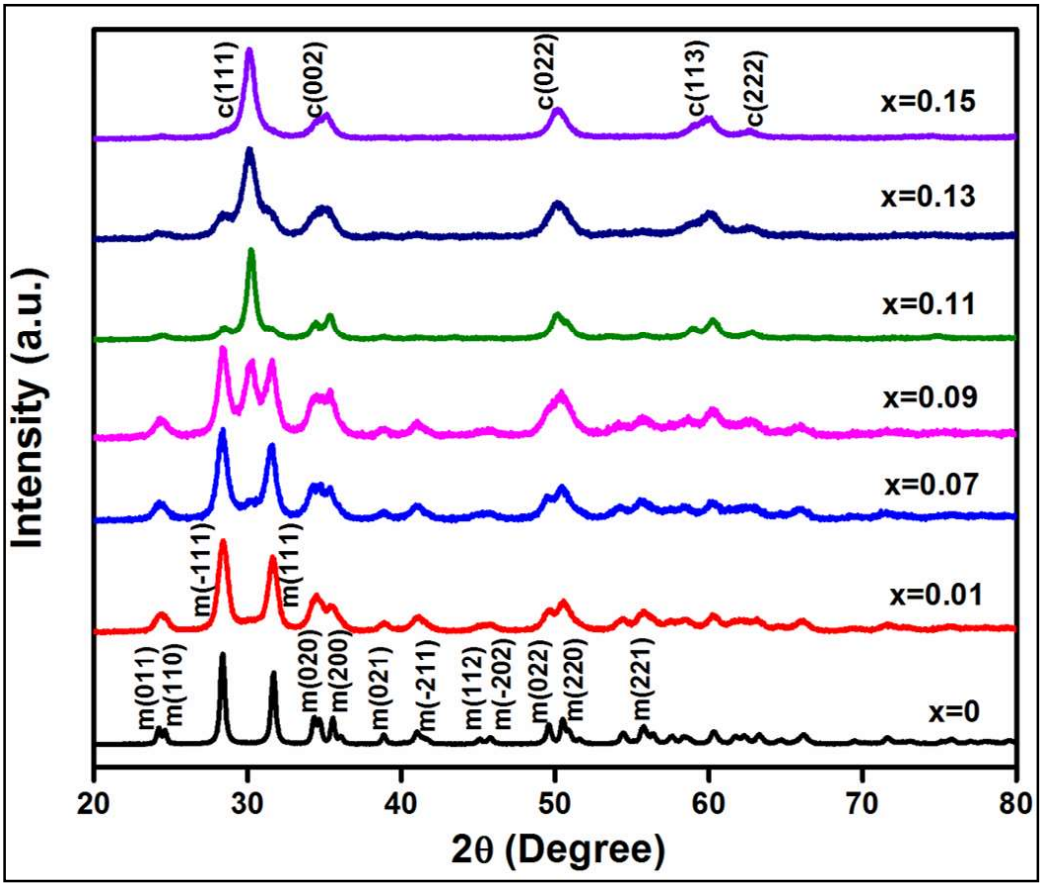

Figure 3.1 *X-ray diffraction patterns of $Hf_{1-x}Pr_xO_2$ ($0 \leq x \leq 0.15$) nanoparticles calcined at 900 °C for 5 hours.*

With increasing Pr concentration, the intensity of (111) plane enhances. At x = 0.07-0.13, the diffraction patterns exhibit peaks corresponding to both monoclinic and cubic phases. Interestingly, the monoclinic phase is fully transformed into a stable cubic phase at x = 0.15. Pr doped HfO_2 nanoparticles do not reveal secondary phase confirming complete substitution of Pr^{3+} at Hf^{4+} sites. The variation of cubic phase fraction with respect to Pr concentration is shown in **Figure 3.2**.

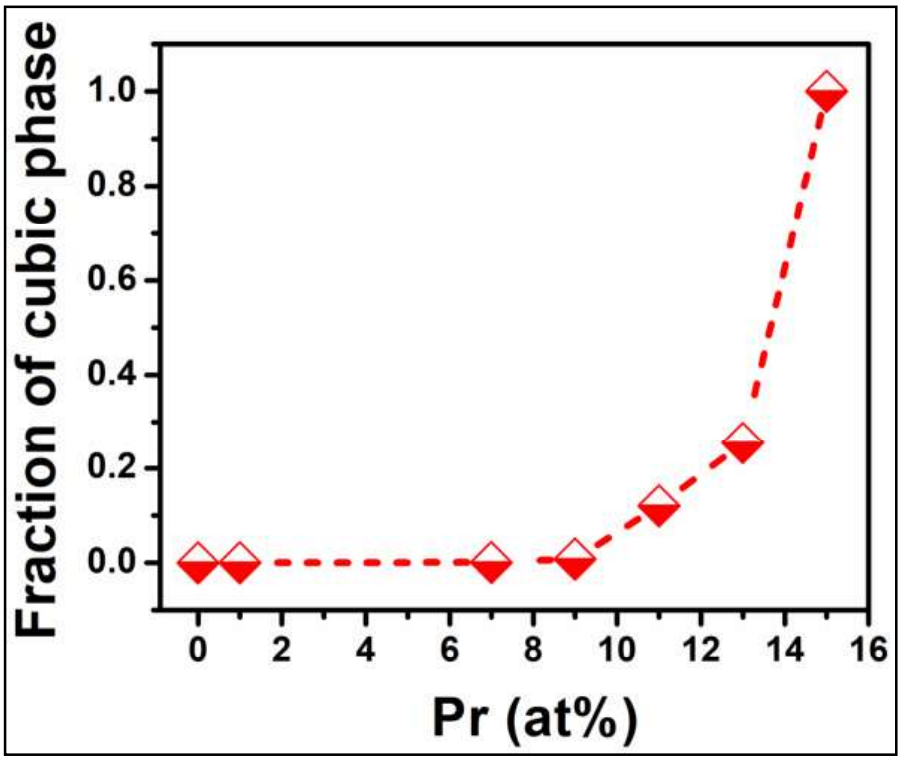

Figure 3.2 *Phase fraction of the cubic phase as a function of Pr concentration.*

In **Figure 3.3**, XRD patterns of x = 0 and 0.15 are well-fitted with $P2_1/c$ and $Fm\bar{3}m$, respectively, using the Rietveld refinement of FullProf software. The fittings provide cell parameters like *a*, *b*, *c* and cell volume as tabulated in **Table 3.1**. The lattice parameters of monoclinic phase are similar to standard values. However, for cubic phase, the lattice parameter enhances from 5.095 to 5.146 Å demonstrating 3% increase in cell volume. The larger cell volume endorses substitution of Hf^{4+} (0.83 Å) with Pr^{3+}ions (1.126 Å). Moreover, the deconvolution of XRD patterns of 11 at% Pr and above reveals that the secondary phase is monoclinic phase only which becomes very weak to absent with increasing Pr concentration.

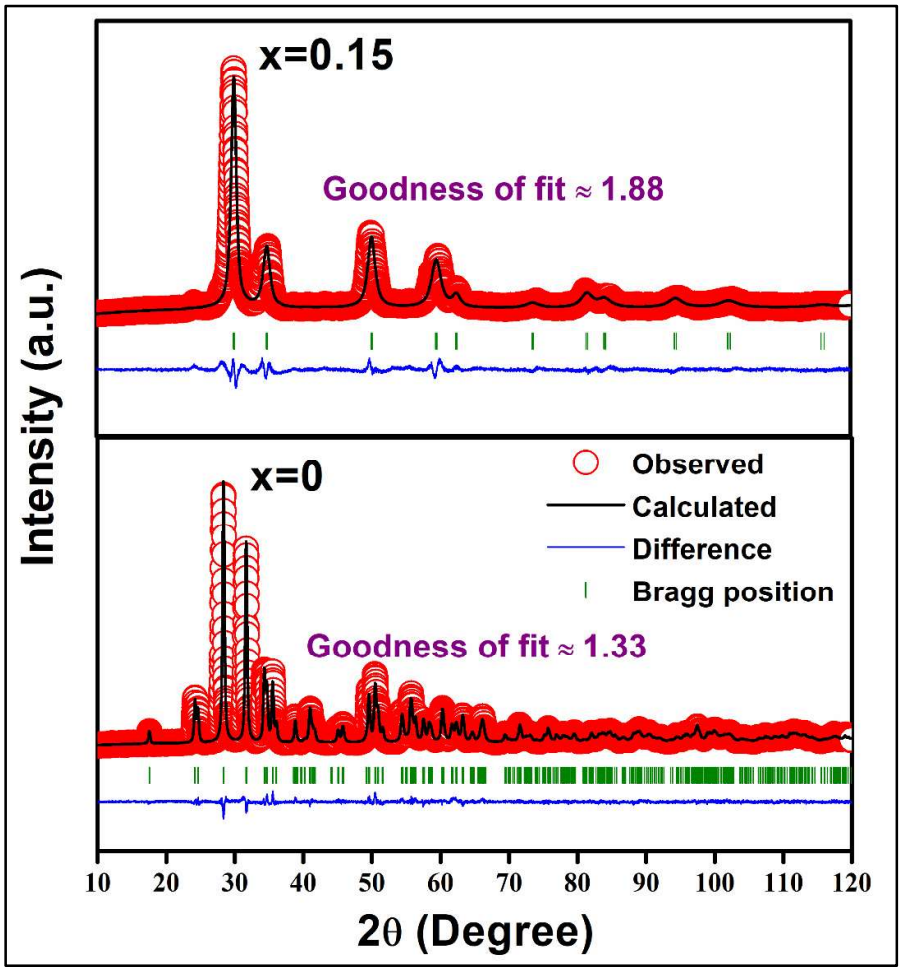

Figure 3.3 *Rietveld refinement of the XRD patterns using FullProf software.*

Table 3.1 *Optimized cell parameters and cell volume for $Hf_{1-x}Pr_xO_2$ (x = 0 and x = 0.15) compared with standard JCPDS data for monoclinic and cubic phase of HfO_2.*

JCPDS card No./ Sample	Crystal structure	Space group	Cell parameters			
			a (Å)	b (Å)	c (Å)	Volume ($Å^3$)
78-0049	Monoclinic	$P2_1/c$	5.117	5.175	5.291	138.32
53-0560	Cubic	$Fm\bar{3}m$	5.095	5.095	5.095	132.26
$Hf_{1-x}Pr_xO_2$ (x=0)	Monoclinic	$P2_1/c$	5.120	5.174	5.295	138.45
$Hf_{1-x}Pr_xO_2$ (x=0.15)	Cubic	$Fm\bar{3}m$	5.146	5.146	5.146	136.25

The significant difference in ionic radii (~ 0.30 Å) induces noticeable lattice strain which is examined by Williamson-Hall (W-H) method as given below:

$$\frac{\beta\cos\theta}{\lambda} = \frac{1}{D} + \frac{\varepsilon\sin\theta}{\lambda} \quad \textbf{(3.1)}$$

where β, θ, ε, D and λ corresponds to full width at half maximum, Bragg angle, strain, crystallite size and X-ray wavelength [129]. **Figure 3.4** demonstrates variation in particle size and lattice strain with increasing Pr concentration. The particle size is estimated as ~ 35 and 10 nm for x = 0 and 0.15, respectively. It is important to note that the drastic reduction in particle size of cubic phase occurs only when strain becomes four times higher compared to monoclinic one. Nevertheless, strain attains the highest value for x = 0.13 containing mixed monoclinic and cubic phase.

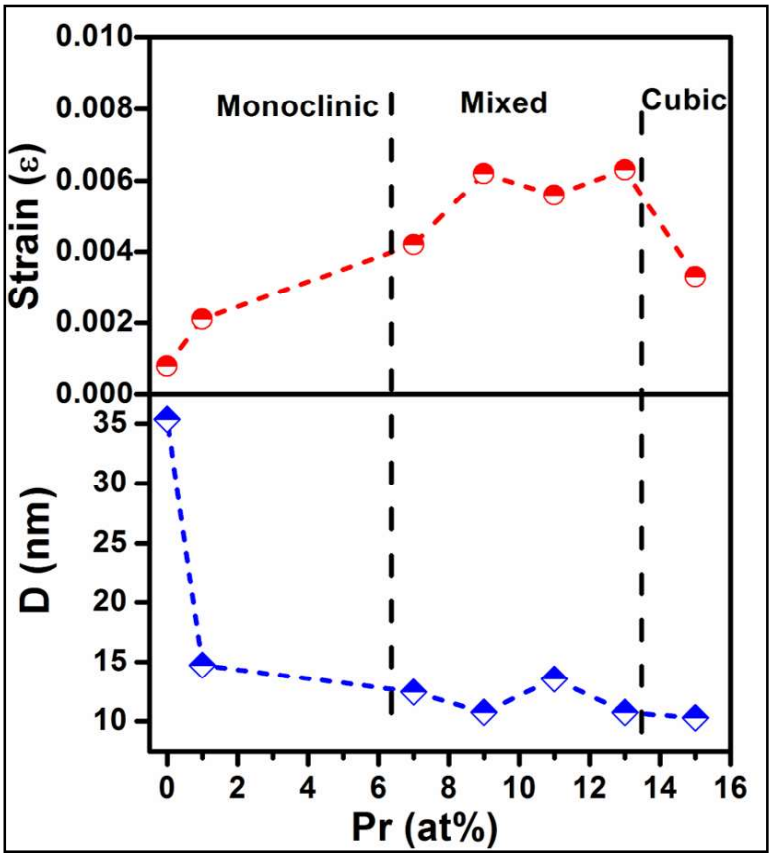

Figure 3.4 *Variation in crystallite size and lattice strain of $Hf_{1-x}Pr_xO_2$ (x = 0-0.15) nanoparticles.*

Further, Raman spectroscopy is used to verify monoclinic and cubic phases of HfO_2. Raman spectra for monoclinic (x = 0) and cubic (x = 0.15) phases of HfO_2 are depicted in **Figure 3.5**. The monoclinic phase contains 18 Raman active modes within the range 100-800 cm^{-1}. While peaks at 257, 336, 383, 498, 581 and 673 cm^{-1} are for A_g vibration modes, the B_g vibration modes are at 243, 324, 398, 521, 551, 640 and 774 cm^{-1} [130]. For cubic phase, a single broadband around 600 cm^{-1} corresponds to breakdown of wave vector selection rule by translational disorder for random substitution of dopant cations and vacancies [131].

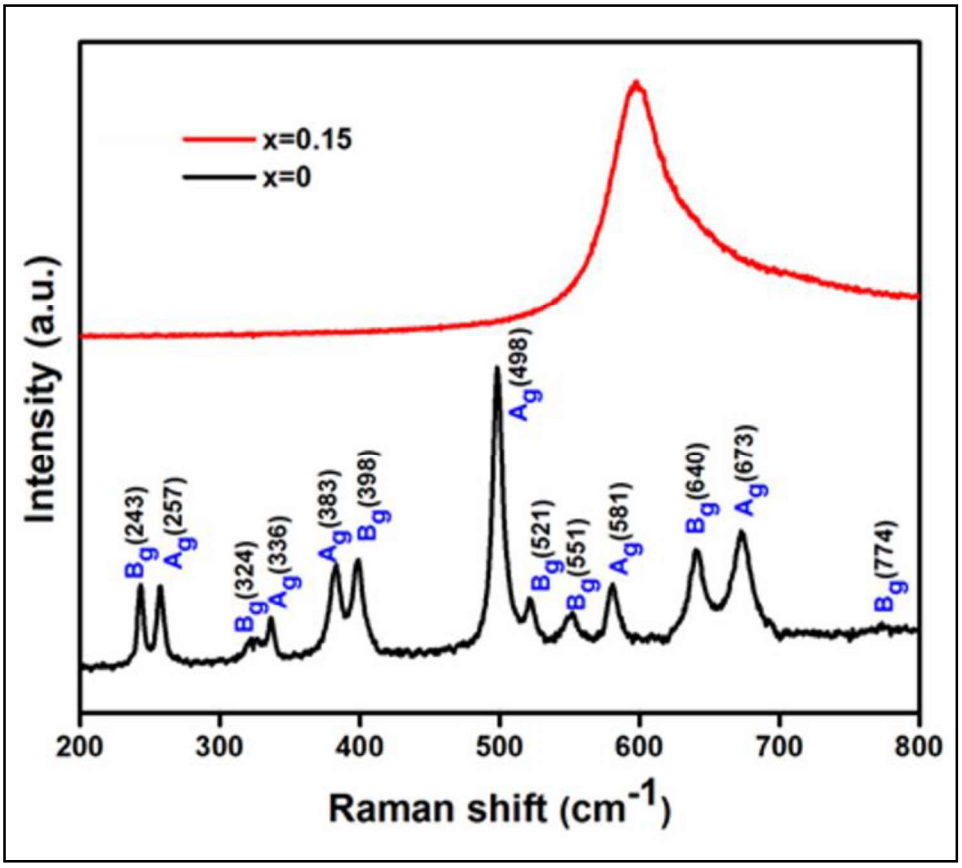

Figure 3.5 *Raman modes monoclinic (x = 0) and cubic (x = 0.15) phase of* $Hf_{1-x}Pr_xO_2$ *nanoparticles.*

Fourier transform infrared (FTIR) spectroscopy is used for the description of organic or inorganic molecules based on the presence of functional groups in the material. FTIR spectra of $Hf_{1-x}Pr_xO_2$ (x = 0, 0.01, 0.09 and 0.15) nanoparticles are given in **Figure 3.6**. The peaks at 520 and 760 cm^{-1} correspond to Hf-O bonds [132]. Another peak at 950 cm^{-1} appears for Hf-OH bonds [133]. While peak at 1374 cm^{-1} belongs to O-C-O symmetric stretching, peak at 1635 cm^{-1} appears for H-O-H bending vibration. However, Pr doping induces distinct band at 2335 cm^{-1} for $^3H_4 \rightarrow {}^3H_5$ transition of Pr^{3+}.

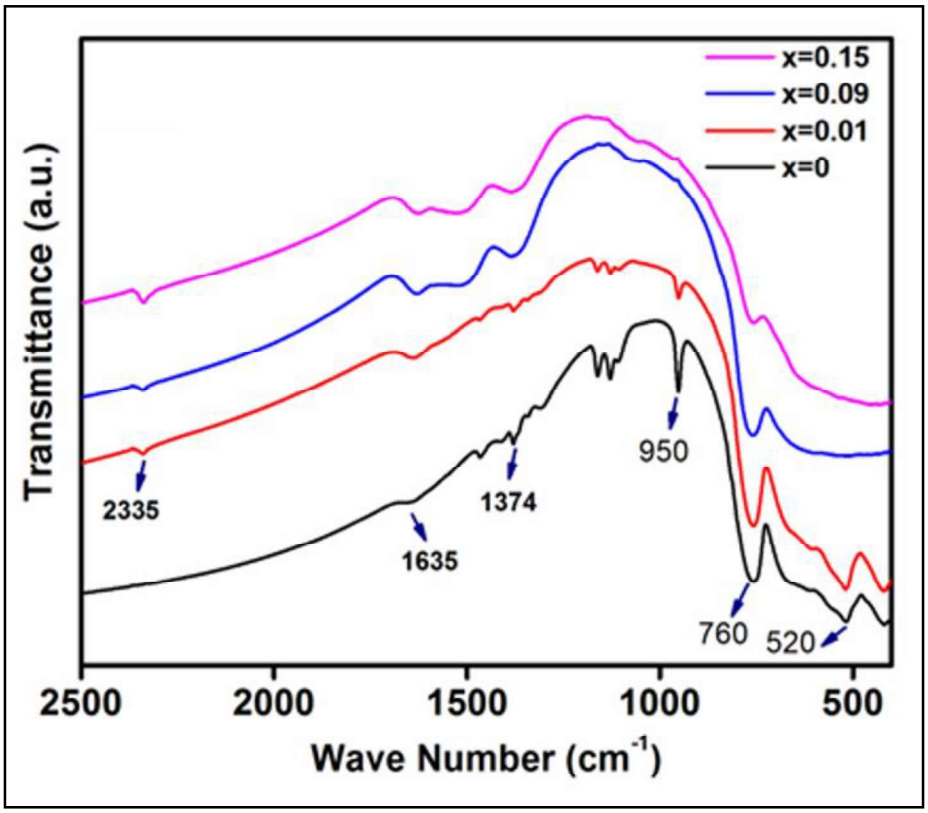

Figure 3.6 *Transmittance spectra of $Hf_{1-x}Pr_xO_2$ nanoparticles (x = 0, 0.01, 0.09 and 0.15) from Fourier transform infrared spectroscopy.*

3.2.2 Microstructural Analysis

Further, the formation of monoclinic and cubic phases is examined by selected area electron diffraction (SAED) patterns for x = 0 and 0.15, as shown in **Figure 3.7 (a)** and **(c)**. The diffraction rings are indexed as (111), ($\bar{1}$11), (002) and ($\bar{2}$12) of $P2_1/c$ in x = 0 and (111), (200), (220) and (311) of $Fm\bar{3}m$ in x = 0.15. The insets of **Figure 3.7 (a)** and **(c)** demonstrate agglomerated and semi-spherical particles whereas particle size distribution histograms confirm average particle size ~ 35 and ~ 11 nm for x = 0 and 0.15, respectively, matching with particle size estimated from W-H plot. In **Figure 3.7 (b)** and **(d)**, high-resolution TEM show inter-planar spacing (d) as ~ 0.281 and ~ 0.182 nm corresponding to (111) and (220) of $P2_1/c$ and $Fm\bar{3}m$, respectively. The high-temperature cubic phase of HfO_2 has been stabilized at room temperature by RE dopants like Dy and Sm, etc. [29,30].

Incorporation of dopants can induce lattice expansion and/or oxygen vacancies (V_o) which play a dominant role. RE ion substituting Hf^{4+} ions produce V_o for charge neutrality. These dopants essentially lower V_o formation energy in HfO_2 lattice [134]. The monoclinic and cubic phase of HfO_2 possesses 7-fold and 8-fold oxygen coordinated Hf^{4+} ions, respectively. Here, Pr doped HfO_2 lattice contains V_o near Hf sites producing 8-fold oxygen coordinated Pr^{3+} ions. At lower Pr concentration, 7-fold oxygen coordinated Hf^{4+} ions are prevalent and hence, monoclinic phase is observed. However, for x = 0.15, 8-fold oxygen coordinated Pr^{3+} ions become sufficient enough to stabilize cubic phase at room temperature.

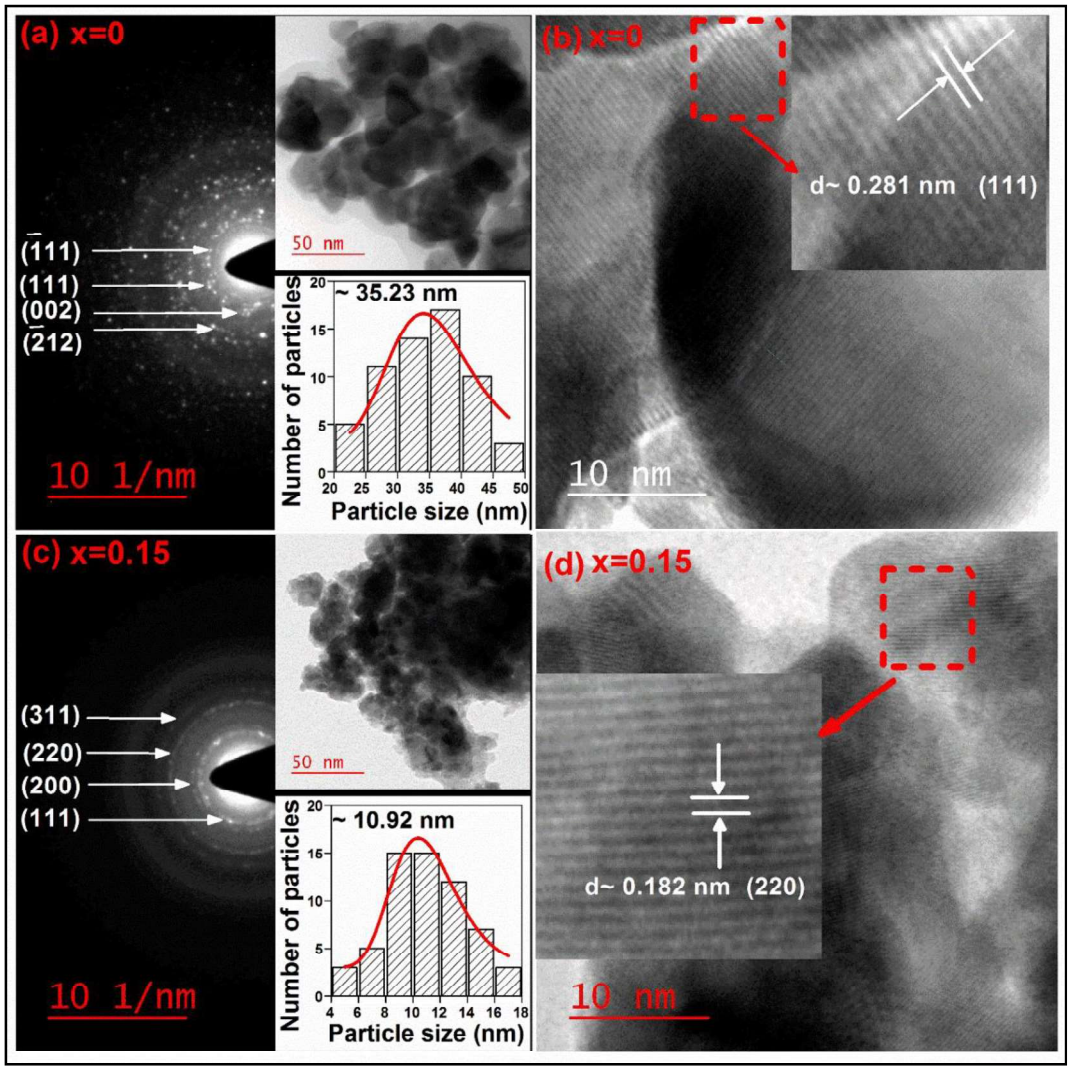

Figure 3.7 *SAED patterns and high-resolution TEM for (a, b) x=0 and (c, d) x=0.15; TEM micrographs and the particle size distribution histograms are shown as the insets of (a) and (c) for respective sample.*

3.2.3 X-ray Photoelectron Spectroscopy

Oxygen vacancy induced phase transformation in Pr doped HfO_2 nanoparticles is examined further through X-ray photoelectron spectroscopy (XPS). XPS spectra for O 1*s* and Pr 3*d* levels of x = 0, 0.09 and 0.15 are shown in **Figure 3.8 (a)** to **(e)**. All peaks are adjusted with respect to C 1*s* peak at 284.6 eV. XPSPEAK 4.1 is used to deconvolute asymmetric spectra. O 1*s* spectra exhibit two peaks at ~ 529 and ~ 530.5 eV marked as

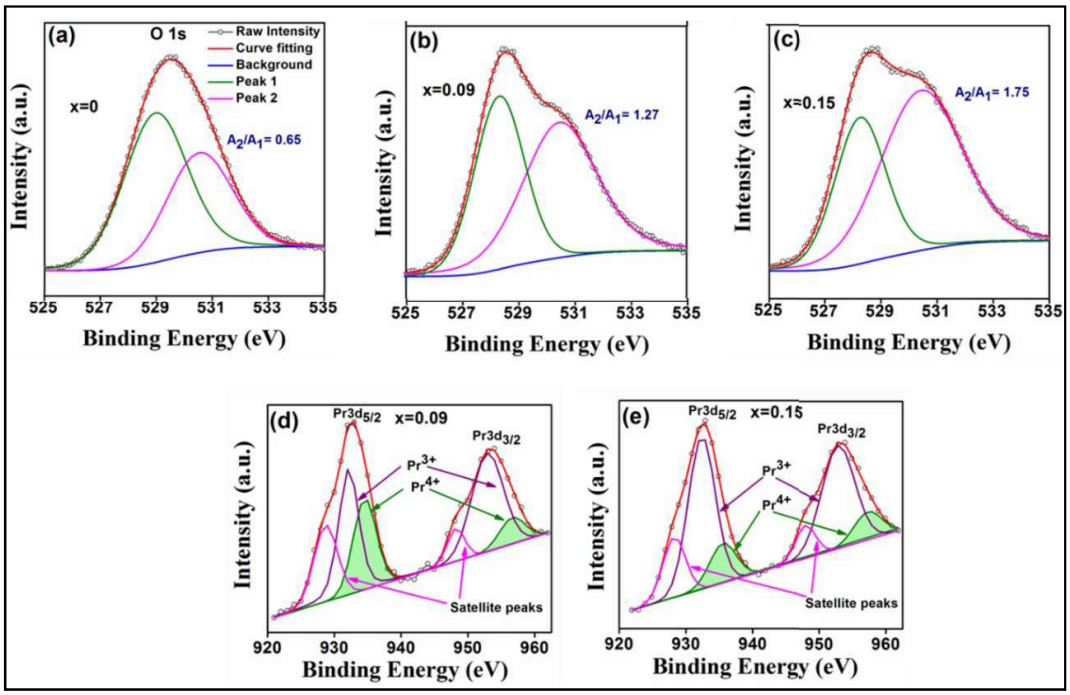

Figure 3.8 *(a), (b), (c) XPS spectra of O 1s and (d), (e) Pr 3d core levels of* $Hf_{1-x}Pr_xO_2$ *nanoparticles.*

peak 1 and 2. The peak with lower binding energy (B.E) demonstrates oxygen in O-Hf^{4+} bond whereas higher B.E peak indicates oxygen deficient regions containing V_o [105]. Comparison of peak area ratio of 2 and 1 (A_2/A_1) reveals that A_2/A_1 enhances with increasing Pr. The meager amount of V_o at the lowest Pr concentration facilitates the monoclinic phase. Gradual increase in Pr concentration (x = 0.07–0.13) reduces V_o formation energy produces more V_o and hence, monoclinic and cubic phase coexists. At x = 0.15, the appropriate V_o concentration stabilizes cubic phase at room temperature. As shown in **Figure 3.9**, Pr 3*d* spectra contain two strong peaks at ~ 932 and 953 eV for $3d_{5/2}$ and $3d_{3/2}$, respectively. The deconvoluted spectra in **Figure 3.8 (d)** and **(e)** indicate that each peak contains three inherent peaks. The peaks at 932.4 eV in $3d_{5/2}$ and at 952.9 eV in $3d_{3/2}$ appear for Pr^{3+} ions and other two peaks (935.5 and 957.3 eV) correspond to Pr^{4+} with shake-off satellites at 928.2 and 948 eV [135]. Pr^{4+} negates V_o formation hindering

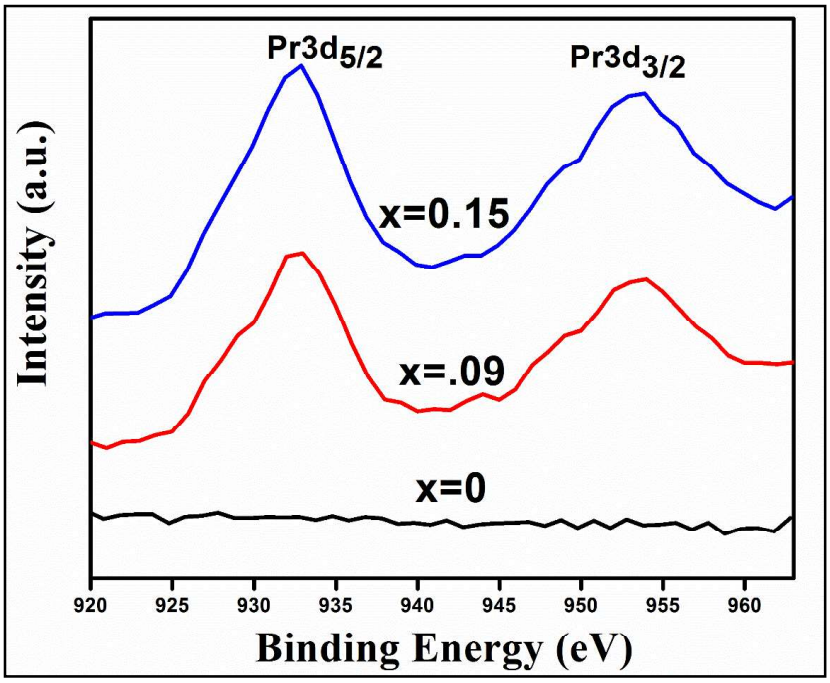

Figure 3.9 *Pr 3d core level spectra of $Hf_{1-x}Pr_xO_2$ (x = 0, 0.09 and x = 0.15) nanoparticles.*

the stabilization of cubic phase. The large amount of Pr^{4+} in x = 0.09 reduces significantly in x = 0.15 that ultimately enhances Pr^{3+} concentration. Thus, in contrast to Dy^{3+} (11 at %) and Sm^{3+} (12 at %), the higher Pr concentration, i.e., 15 at %, is required to stabilize the cubic phase at room temperature. Moreover, the actual percentage of Pr dopant is estimated as 8.8 and 14.3 for the 9 and 15 at% dopant feed ratios from the intensity ratio of Hf and Pr observed from the XPS spectra.

3.2.4 Mechanism for Phase Transformation from Monoclinic to Cubic

Bulk HfO_2 possesses different polymorphs such as monoclinic, tetragonal and cubic phase. While monoclinic phase is stable at room temperature, HfO_2 undergoes a phase transition to the tetragonal and cubic phase at ~ 1700 and ~ 2600 °C, respectively. According to previously reported literature, the stabilization of the high temperature cubic phase of HfO_2 at room temperature can be achieved by incorporating dopants such

as Mn, Ce, Lu and Y with different charge states [136–139]. In this context, the high temperature cubic phase of HfO_2 is stabilized at room temperature by incorporating Dy and Sm up to 11 and 12 at%, respectively. Gao *et al.* report the synthesis of Mn doped HfO_2 nanoparticles through a solid-state reaction method and demonstrate the stabilization of the cubic phase within a narrow composition range of 20-30% of Mn [136]. It has been revealed that the monoclinic to cubic phase transformation involves the combined effect of size of Mn ion and charge states. Gálvez-Barboza *et al.* have achieved the cubic phase in 10 wt% Ce doped HfO_2 synthesized by a modified sol-gel technique [137]. Matović *et al.* report the stabilization of the cubic phase of HfO_2 at room temperature after doping 20 mol% of yttrium [139].

Recently, in our group, we have shown that by incorporating Dy up to 11 at% and Sm up to 12 at%, the monoclinic phase of HfO_2 transforms to the high temperature cubic phase which remains stable at room temperature [29,30]. The stabilization of the cubic phase is ascribed to the formation of oxygen vacancies generated by the substitution of Dy^{3+}/Sm^{3+} ions at Hf^{4+} ion site. It is supported by the first principle calculation which predicts that when a trivalent dopant cation substitutes Hf^{4+} ion, the deficiency of electrons in the host lattice occur and results in the formation of oxygen vacancies (V_o) due to charge compensation [61,140]. The concentration of oxygen vacancies varies with increase in trivalent dopant concentration. The incorporation of trivalent dopants in HfO_2 lattice leads to reduction in the formation energy to produce an oxygen vacancy. It is well known that in monoclinic HfO_2, the coordination number of Hf^{4+} cation is 7, whereas the coordination number in high symmetry cubic phase of HfO_2 is 8 [61]. In the present case, when the Pr^{3+} ions having a lower charge state and a larger ionic radius, replace Hf^{4+} ions, the oxygen vacancies are generated which prefer to reside near Hf atoms and leave 8-fold oxygen coordination to Pr^{3+} ions in the host lattice. When Pr^{3+} ion concentrations are low,

due to insufficient amount of oxygen vacancy, HfO_2 exhibits the monoclinic phase and Hf is covalently bonded with O favoring 7-fold Hf coordination. With increase in Pr concentration, the energy needed to form an oxygen vacancy significantly decreases. As a result, a mixed phase of the monoclinic and cubic is observed for $0.07 \leq x \leq 0.13$. When a sufficient number of Pr^{3+} ion forming an 8-fold coordination with oxygen ion are present in the lattice, the high temperature cubic phase of HfO_2 becomes stable even at room temperature. At x = 0.15, there exists a nominal concentration of oxygen vacancies associated to Hf cation resulting in an 8-fold oxygen coordination to Pr^{3+} ions that surpass the 7-fold Hf coordination, thereby stabilizing the cubic phase at room temperature.

3.3 Optical Properties: Bandgap Estimation

Figure 3.10 shows UV-visible absorption spectra for x = 0, 0.09, 0.15. In x = 0, the peak at ~ 264 nm corresponds to absorption band of HfO_2. No absorption peak is realized in visible region. For x = 0.09 and 0.15, along with peak at ~ 264 nm, another peak emerges at ~ 736 nm for transition, $^3P_0 \rightarrow {}^3F_4$ of Pr^{3+}.

The values of optical bandgap (E_g) are determined as follows:

$$\alpha = \frac{A(h\nu - E_g)^{1/2}}{h\nu} \qquad (3.2)$$

where α, $h\nu$ and A are absorption coefficient, photon energy and proportionality constant, respectively [141]. The band gap values are found to be 5.42, 5.05 and 5.06 eV for x = 0, 0.09 and 0.15, respectively (**Figure 3.11**). The estimated band gaps agree well with the reported one [142]. After incorporating Pr, E_g decreases due to surplus of defect states forming sub-bands near conduction band. Moreover, the alloying effect of HfO_2 and non-stoichiometric HfO_{2-x} also contribute towards the narrowing of the bandgap [143].

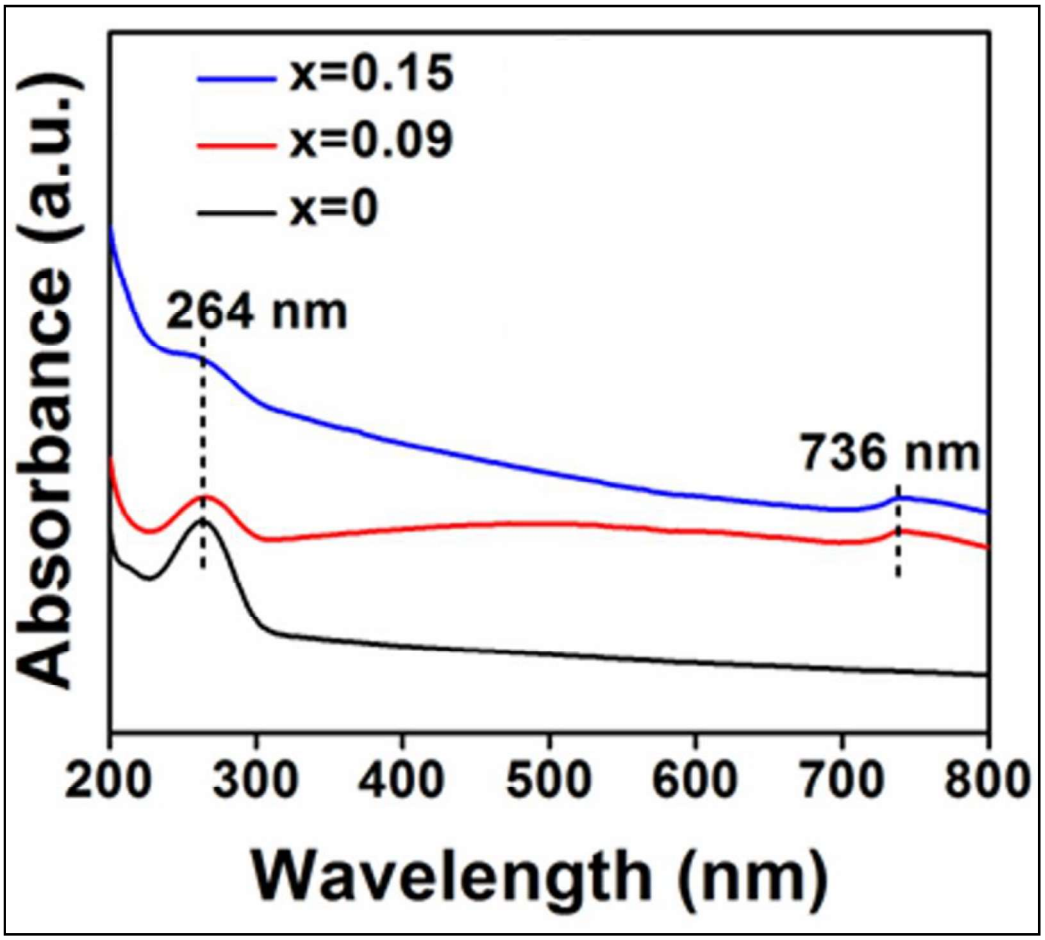

Figure 3.10 *UV-visible absorption spectra of $Hf_{1-x}Pr_xO_2$ (x = 0, 0.09 and 0.15) nanoparticles.*

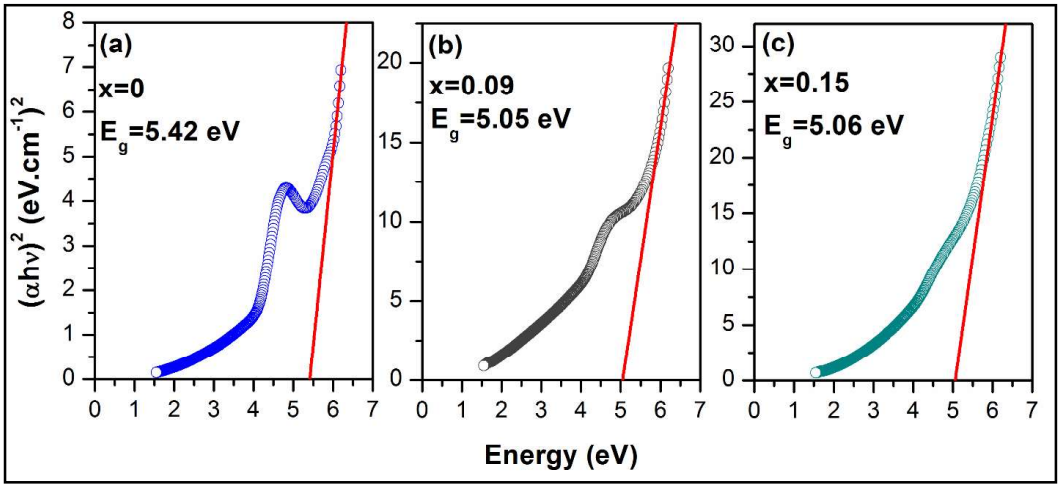

Figure 3.11 *Tauc plots of $Hf_{1-x}Pr_xO_2$ nanoparticles (a) x = 0, (b) x = 0.09 and (c) x = 0.15.*

The lattice strain decreases in 15 at% Pr doped HfO_2 compared to 9 at% Pr doped HfO_2, while the number of oxygen vacancies is higher in the 15 at% Pr doped HfO_2. Due to the competition between lattice strain and oxygen vacancy concentration, the bandgap of 15 at% Pr doped HfO_2 is almost the same as that of 9 at% Pr doped HfO_2 [144].

3.4 Conclusions

In this chapter, we investigated the monoclinic to high-temperature cubic phase transformation after incorporating 15 at% of Pr. The monoclinic phase was observed below 7 at% of Pr followed by a mixed phase at intermediate Pr concentrations. The combined analysis of Rietveld refinement, Raman spectra, FTIR spectra, SAED patterns and high-resolution TEM confirmed the monoclinic and cubic phases. Williamson-Hall analysis revealed a reduction in particle size from ~ 35 to 10 nm with enhanced lattice strain and cell volume due to mismatched ionic radii of Pr^{3+} and Hf^{4+}. XPS study demonstrated that the substitution of Pr^{3+} with Hf^{4+} introduced more oxygen vacancies which formed 8-fold oxygen coordinated Pr^{3+} ion, thereby stabilizing the cubic phase at room temperature. While HfO_2 exhibited a bandgap of ~ 5.42 eV, after doping 15 at% of Pr, the bandgap reduced to ~ 5.06 eV due to the alloying effect of HfO_2 and the formation of sub-bands near the conduction band.